fibers

MDPI

Article

Exploration of Wave Development during Yarn Transverse Impact

Matthew Hudspeth [1,†], Emily Jewell [2], Suzanne Horner [3], James Zheng [3] and Weinong Chen [1,4,*]

1 School of Aeronautics and Astronautics, Purdue University, West Lafayette, IN 47907, USA
2 Indiana University School of Medicine, Indiana University, Indianapolis, IN 46202, USA
3 Program Executive Office – Soldier, US Army, Fort Belvoir, VA 22060, USA
4 School of Materials Engineering, Purdue University, West Lafayette, IN 47907, USA
* Correspondence: wchen@purdue.edu; Tel.: +1-765-494-1788
† Current address: Currently with Sandia National Laboratories, Albuquerque, NM 87123, USA.

Academic Editor: John W. Gillespie
Received: 5 December 2016; Accepted: 24 April 2017; Published: 16 May 2017

Abstract: Single yarns have been impacted in a transverse fashion so as to probe the characteristics of resulting wave development. Longitudinal wave speeds were tracked in efforts to directly measure the yarn tensile stiffness, resulting in a slight increase in the modulus of Kevlar® KM2 and Dyneema® SK76. Additionally, the load developed in AuTx® and Kevlar® KM2 yarns behind the longitudinal wave front has been recorded, providing additional verification for the Smith relations. Further effort to bolster the Smith equations has been successfully performed via tracking transverse wave speeds in AuTx® yarns over a range of impacting velocities. Additional emphasis has been placed at understanding the transverse wave development around the yarn critical velocity, demonstrating that there is a velocity zone where partial yarn failure is detected. Above the critical velocity, measurement of early time transverse wave speeds also agrees with the Smith solution, though the wave speed quickly reduces in value due to the drop in tensile stresses resulting from filament rupture. Finally, the Smith equations have been simplified and are compared to the Cunniff equation, which bear a striking resemblance. Due to such a resemblance, it is suggested that yarn critical velocity experiments can be performed on trial yarn material, and the effect of modifying yarn mechanical properties is discussed.

Keywords: Kevlar®; Dyneema®; transverse impact; projectile; wave speed; Cunniff velocity; critical velocity

1. Introduction

Although a rather uncommon experiment, transverse impact into single yarns has been historically used to determine baseline yarn mechanical properties, specifically to determine yarn stiffness in the longitudinal direction and the yarn critical velocity, wherein the material fails "instantly" upon projectile-yarn contact [1–10]. Such an understanding of stiffness and critical velocity is used to assess the efficacy of implementing a specific yarn material into a full body armor system; an efficacy analysis is most reasonably performed by determining the Cunniff parameter ($\Omega^{1/3}$) [11], which is described in Equation (1),

$$\Omega^{1/3} = \left(\frac{\sigma \epsilon}{2\rho} \sqrt{\frac{E}{\rho}} \right)^{1/3} \tag{1}$$

wherein σ, ϵ, E and ρ represent the longitudinal failure strength, longitudinal failure strain, longitudinal elastic modulus and density, respectively. The Cunniff parameter, an astute empirical relation developed from non-dimensional analysis of extensive experimental study, can be best thought of as

the product of the yarn specific toughness and the longitudinal wave speed; essentially, it is desirable to maximize the energy absorbed by the constituent yarns before rupture and to move this energy away from the impact site as quickly as possible. Thus, maximizing strength, strain and stiffness, while decreasing density, are key parameters required to increase the halting capability of a fabric system. Further analysis into the coupling of the first three parameters is discussed in Section 4.

Understanding the Cunniff parameter unveils the power available in performing single yarn impact experiments. Not only are yarn experiments much more cost effective to perform on novel materials as compared to full fabric experiments, it is indeed possible to determine the failure strength, failure strain and elastic modulus developed during the single-yarn impact event. Each of the aforementioned mechanical properties can be directly input into the Cunniff parameter, thereby allowing comparison of various yarn types in an impact environment, creating similar loading conditions to that seen from full fabric impact. It must be noted that traditional predictions of the Cunniff parameter generally rely upon quasi-static mechanical properties, but as was shown by Hudspeth et al. [12], care must be taken to understand the projectile loading conditions exhibited on the yarn of interest.

Having provided an explanation for the need to ascertain input values for the Cunniff parameter described in Equation (1), it is now of interest to briefly overview the governing mechanics of transverse impact of a projectile into a single yarn in efforts to provide a background on the deformation behavior and resulting system response. Upon impact, a longitudinal tensile wave emanates away from the projectile-yarn contact site, moving at the longitudinal speed of sound in the material, c, being described by Equation (2), where E and ρ represent the longitudinal tensile modulus and the material density, respectively.

$$c = \sqrt{\frac{E}{\rho}} \tag{2}$$

Material behind the longitudinal wave front is set in tension, moving inward toward the projectile-yarn contact site with a particle velocity of W, which is described by Equation (3), wherein ϵ signifies the strain amplitude developed due to the passing of the longitudinal wave.

$$W = c\epsilon \tag{3}$$

In addition, a transverse wave is also developed upon the projectile-yarn contact, following behind the longitudinal wave, and possesses the wave velocity U, being described by Equation (4), or in the laboratory reference frame, as U_{obs}, being described by Equation (5).

$$U = c\sqrt{\frac{\epsilon}{1+\epsilon}} \tag{4}$$

$$U_{obs} = c\left(\sqrt{\epsilon(1+\epsilon)} - \epsilon\right) \tag{5}$$

Material behind the transverse wave front transitions from an inward velocity (perpendicular to the projectile direction) to a particle velocity identical in magnitude and direction to that of the projectile, being described by Equation (6). U differs from U_{obs} in that the reference frame of the former is attached to the inward flowing yarn material and the latter is attached to an external viewer. Solving Equations (2)–(6) allows for determination of the strain developed in the yarn at a specific impacting velocity, V, or vice versa, one can solve for the velocity required to initiate a specific strain value, ϵ.

$$V = \sqrt{(1+\epsilon)^2U^2 - ((1+\epsilon)U - W)^2} \tag{6}$$

Finally, Equation (7) can be used to solve for the angle θ developed behind the transverse wave front, which notably remains constant during the impact event, barring rarefaction waves emanating from yarn-end boundaries.

$$\theta = tan^{-1}\left(\frac{V}{U(1+\epsilon) - W}\right) \tag{7}$$

The validity of Equations (2)–(7) is reasonably well substantiated by experimental evidence from various authors; the reader is directed to Hudspeth et al. [12] for a thorough list of previous authors who use the single yarn transverse impact experiment to gain understanding of yarn mechanical properties, most notably the yarn critical velocity. The reader is specifically directed to work performed by Chocron et al. [10] and Chocron and Walker [13], who take great effort in determining the critical velocity for several types of high-performance yarn. Additionally, Walker and Chocron [13] present a strong explanation for the oft-quoted difference between experimental and theoretical critical velocities predicted by Equations (2)–(6). Additional explanation regarding the experimental/theoretical variation in critical velocity has also been given by Carr [8], Bazhenov et al. [9], Sockalingam et al. [14] and Hudspeth et al. [12,15].

The current experimental dataset was analyzed in an effort to determine the presence of a rate sensitivity for both Kevlar® KM2 and Dyneema® SK76, but concurrent efforts also led to experiments analyzing the validity of the strain state developed behind the longitudinal wave front and determination of the transverse wave velocity, with both sets of latter experiments being performed on AuTx® yarn. Finally, due to the nature of determining the *in situ* mechanical properties of these materials (along with data from [12]), it is of interest to assess the effect of varying stress, strain and modulus in efforts to achieve greater transverse critical velocities, which will be discussed in Section 4. As previously mentioned, this variation of mechanical properties has also been expanded to briefly assess their effect on the oft-quoted Cunniff parameter.

2. Experimental Section

2.1. Materials

Three different high performance yarn materials have been used to assess both the longitudinal and transverse stress wave characteristics, namely Dyneema® SK76, Kevlar® KM2 and AuTx®. Quasi-static mechanical properties of all said fibers are displayed in Table 1. Dyneema® SK76 and Kevlar® KM2 yarns were selected as candidate materials due to their regular occurrence within current body armor systems, while AuTx® yarn was selected as it is a prospect for future armor systems. Yarns were impacted with three different projectile nose geometries, namely razor blade, 0.30-caliber (cal) fragment simulating projectile (FSP) and 0.30-cal round. An image of the three different projectile heads can be found in Figure 1. Further description of the experimental setup and procedures can be found in Hudspeth et al. [12].

Table 1. Yarn quasi-static mechanical properties. Note: Mechanical property data have been taken from single yarn tension experiments using a 666-mm gauge length [15].

Fiber Type	Kevlar® KM2	Dyneema® SK76	AuTx®
Linear Density (denier)	600	1350	275
Failure Strain (%)	2.56	2.65	2.87
Failure Stress (GPa)	2.52	2.81	2.99
Elastic Modulus (GPa)	100.2	129.3	129.9

Figure 1. Projectiles used for transverse impact into yarn material. From left to right can be seen the 0.30-cal round, 0.30-cal FSP and razor blade projectiles [12].

2.2. Longitudinal Wave

In order to determine the presence of a rate sensitivity of high-performance fiber in a transverse impact environment, the velocity of the longitudinal wave fronts developed upon projectile-yarn contact was tracked in situ. Initially, it is valid to assess the yarn wave speed, c, via determining the time required for the longitudinal wave to travel from the contact site to the yarn grip, which has been mounted onto a fast-response force transducer. This simple method is described by Equation (8), where L represents the distance from the projectile contact site to the yarn clamp, and t represents the duration between the time of impact to the time of arrival of the longitudinal wave to the yarn clamp.

$$c = \frac{L}{t} \tag{8}$$

High speed imaging has been used to track yarn deformation and failure during the impact event, which ideally, could give an impact time, but it must be noted that it is impossible to know the actual time of impact of the projectile into the yarn, as contact will always be made at some inter-frame separation or during a frame exposure. Thus, while estimating the impact time using imaging would be appropriate with sufficient framing rates, low frame rates (e.g., older camera systems) result in inter-frame separation great enough to skew the initial impact time, resulting in insufficient error bounds being placed on the measured wave velocity. As such, estimating the time of impact has been avoided in lieu of an alternative measurement approach, namely using the arrival times of the longitudinal wave fronts at two ends of the yarn that have a large offset between the yarn mid-length and the actual contact site. An example of this offset impact geometry can be seen in Figure 2. In this specific geometry, it is possible to accurately determine the location of impact with a reasonably high level of accuracy using a laser bore site inserted into the muzzle of the barrel. Measuring from the clamp locations to the location demarcated by the laser yields both lengths L_1 and L_2. The wave velocity c can then be determined using Equation (9) if one knows the difference in arrival times of the two emanating longitudinal waves meeting their respective clamping boundaries, being denoted as t_1 and t_2, respectively. A similar technique has also been employed by an oft-quoted yet elusive study by Wang et al. [16].

$$c = \frac{L_1}{t_1} = \frac{L_2}{t_2} \tag{9}$$

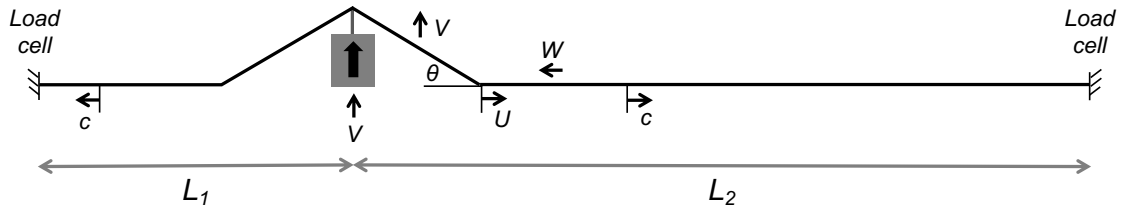

Figure 2. Schematic of single yarn transverse geometry used to determine longitudinal wave speeds.

As previously stated, without sufficient framing rates, both t_1 and t_2 can only be estimated with a low level of precision. In order to circumvent this high variability measurement, a more appropriate method has been pursued wherein one tracks the difference in longitudinal wave travel times from projectile-yarn contact site to the detection of the longitudinal wave from the clamping load cells for drastically different yarn lengths L_1 and L_2; L_1 and L_2 are measured as 10.3 cm and 73.2 cm, respectively. Such a measurement is described in Equation (10) and is demonstrated in Figure 3. As previously stated, possessing accurate L_1 and L_2 is achieved using a laser bore site, allowing for Equation (10) to provide an accurate estimate of the wave speed of the yarn material. As an aside, it is important to note that the longitudinal stress wave must also travel through the yarn clamping fixtures, but accounting for this travel time is unnecessary if identical clamping fixtures are used on both ends of the yarn; the longitudinal wave travel time through the clamps is identical in both fixtures and is inherently subtracted out using the aforementioned time difference method. Additionally, the time origin in Figure 3 is arbitrary, and time zero has been set to the instant the data collection system is triggered; thus, a rough calculation of the projectile impact time is -20 µs to 41.5 µs within Figure 3, including wave travel through yarn and clamp.

$$c = \frac{L_2 - L_1}{\Delta t} \tag{10}$$

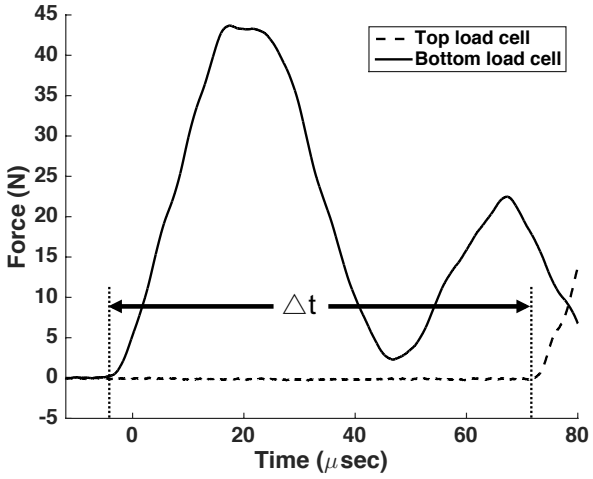

Figure 3. Representative load cell history measured during an impact event.

Finally, due to the presence of the aforementioned load cells onto which the yarn clamps were attached, it was feasible to track the load developed in the yarn behind the longitudinal wavefront. Specifically, effort was placed on determining the stress developed in the yarn as a comparison to the analytical evaluation of strain described in Equations (2)–(7). Results from razor blade transverse impact were analyzed for both Kevlar® KM2 and AuTx® yarns. It is important to note that although the maximum load detected by the transducers does indeed represent the max load generated by the

longitudinal stress wave, the temporal load evolution depicted by the force transducers is not identical to that present in the actual fiber, due to the inertial presence of the yarn clamp; caution is advised when analyzing the load history in Figure 3, as a reader may initially believe it is possible to assess a strain rate from the slope of the force history plot. The quantity of interest from this dataset is based on the max load amplitude and, for example, in Figure 3 is roughly 44 N. Additionally, it is important to note that the force values measured in the load cells are roughly twice that generated in the wake of the longitudinal wave, due to the wave reflection from the rigid clamp boundary. As such, the measured load values used for analysis of Equation (2) result from maximum detected load amplitudes that have been appropriately halved to represent the load that would be developed behind the longitudinal wave front before interaction with the rigid clamping boundary.

2.3. Transverse Wave

Along with determining the effect of impact velocity on the longitudinal wave speed, it was also deemed of use to assess the transverse wave velocity as a function of impact velocity. This transverse wave, which is described by Equation (4) in Section 1, presents itself in a tent formation, thereby allowing direct tracking of wave velocity using high-speed imaging. An example of this transverse wave movement can be seen in the schematic shown in Figure 4. Specifically, attention was placed on movement of the transverse wavefront between several frames, and in tandem with known inter-frame separations, observed transverse wave velocities were calculated for various impacting velocities.

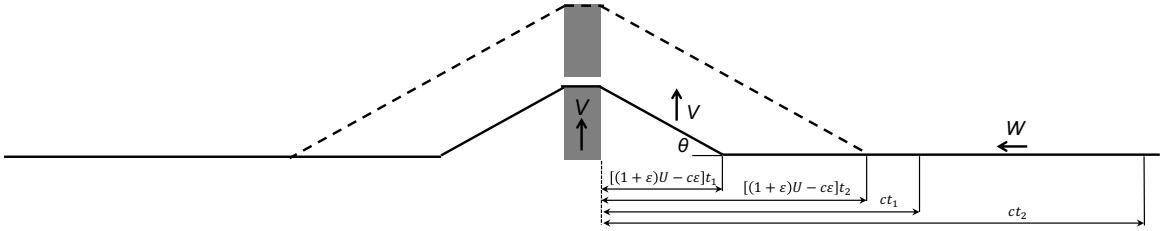

Figure 4. Longitudinal and transverse wave front positioning at two instances in time post impact.

3. Results and Discussion

3.1. Longitudinal Wave

3.1.1. Wave Speed

As described in Section 2.2, longitudinal wave speeds have been tracked for a number of transverse impact experiments for Dyneema® SK76 and Kevlar® KM2. A table describing wave speeds and corresponding elastic moduli can be found in Table 2, and a plot of the experimentally-measured longitudinal wave speed as a function of impacting velocity can be seen in Figure 5.

Transverse impact experiments performed on Dyneema® SK76 yarn resulted in longitudinal wave speed values of 11,466 ± 795 m/s, 12,416 ± 342 m/s and 12,332 ± 262 m/s, when impacting with razor blade, FSP and round projectile geometries, respectively. Average impacting velocities for the razor blade, FSP and round projectile into the Dyneema® yarn were measured as 357 m/s, 547 m/s and 619 m/s, respectively. Although small, it is suggested that the variation in measured wave speed could arise due to projectile contact site inconsistency, with one standard deviation in the measured wave speed resulting in a contact site variation of roughly 2–7 mm. Though plausible, such a large shot line deviation is not seen in any of the high-speed images. An alternative explanation can also be postulated that yarn entanglement, be it due to sizing or yarn twist, could alter the nature of the perceived linear density of the yarn, thereby affecting the longitudinal sound velocity.

From Figure 5a, it can also be seen that there may exist a slight increase in longitudinal wave velocity with increasing transverse impact speeds. Such a slight rate sensitivity is not uncommon in ultra high molecular weight polyethylene (UHMWPE) fiber, and an example is given by Cansfield et al. [17], who showed a linear increase in failure stress with a logarithmic increase in applied strain rate from strain rates ranging from 10^{-4} s^{-1}–10^{-1} s^{-1}. Finally, it is important to note that the elastic modulus exhibited by these fibers at such an elevated strain rate has been determined to be roughly 128 GPa, 150 GPa and 148 GPa when using the razor blade, FSP and round indenters. If there is indeed an increase in longitudinal wave speed, there is a likewise increase in elastic modulus; it must though be noted that the scatter measured in the longitudinal wave speed makes it impossible to affirm the rate sensitivity of the yarn material. Additionally, it is highly doubtful the projectile nose geometry plays any role on the longitudinal wave speed; rather, the three different geometries used for the current experiments were shot generally in different velocity regimes, as these experiments were primarily performed in order to determine the yarn critical velocity, as described in Hudspeth et al. [12]. It could also be argued that partial yarn failure could cause a slowing of the yarn wave speed if non-tensioned filaments provide a pseudo-density increase due to yarn entanglement, but such an argument appears unlikely as the longitudinal wave speed does not decrease when impacting within the critical velocity transition regime for each projectile nose geometry. This lack in variation of longitudinal wave speed when impacting with a specific nose geometry is also bolstered by the consistency of the observed initial transverse wave velocity below, within and above the critical velocity transition regime, which will be demonstrated in Section 3.2.

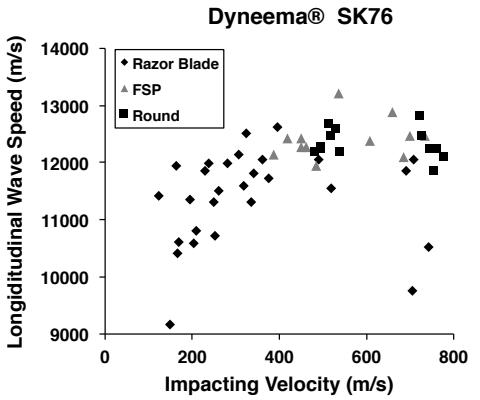

(a)

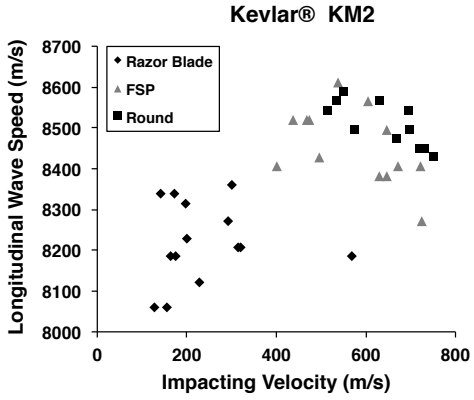

(b)

Figure 5. Measured longitudinal wave speeds of (**a**) Dyneema® SK76 and (**b**) Kevlar® KM2 when impacted with razor blade, FSP and round projectiles.

As demonstrated in Figure 5b, longitudinal wave speeds for Kevlar® resulted in values of 8182 ± 128 m/s, 8454 ± 93 m/s and 8505 ± 53 m/s, for the razor blade, FSP and round projectile geometries, respectively. Average impact velocities for the razor blade, FSP and round projectiles into the Kevlar® yarn were measured as 212 m/s, 573 m/s and 643 m/s, respectively. Similar to the explanation given for impact into Dyneema® yarns, it is suggested that the variation in wave speed may have arisen due to a slight projectile contact site variation, with one standard deviation in the measured wave speed resulting in a variation of roughly 1 mm.

Again, similar to the Dyneema® yarns, Kevlar® also may exhibit a slight degree of material rate sensitivity, although if present, much less pronounced in Kevlar® as compared to Dyneema®. Using the experimentally-measured wave speeds exhibited by these fibers at such an elevated strain rate, calculation of the elastic modulus from Equation (2) results in values of roughly 96 GPa, 101 GPa and 103 GPa when using the razor blade, FSP and round indenters, respectively. This slight increase in modulus, as just mentioned, may occur due to the increase in impacting velocity ranges of each projectile, thereby increasing the strain rate at which the filaments are loaded in tension. That said, it must be noted that such a rate sensitivity is quite small and well within the variance demonstrated by the series of experiments. Additionally, it must be noted that said rate sensitivity was not found by Wang et al. [16] when impacting Kevlar® 29 and Spectra® 1000, presumably due to the small range of impact velocities (80–170 m/s).

Table 2. Longitudinal wave speeds and resulting moduli for both Dyneema® SK76 and Kevlar® KM2.

Fiber Type	**Kevlar® KM2**			**Dyneema® SK76**		
Projectile	Razor Blade	FSP	Round	Razor Blade	FSP	Round
Impact Velocity – Avg (m/s)	211	573	643	357	547	619
Longitudinal Wave Speed – Avg (m/s)	8182	8454	8505	11,466	12,416	12,312
Longitudinal Wave Speed – SD (m/s)	128	93	53	795	342	262
Elastic Modulus – Avg (GPa)	96	103	104	128	150	148
Elastic Modulus – SD Low (GPa)	93	101	103	110	141	141
Elastic Modulus – SD High (GPa)	99	105	105	146	158	154

Note: Avg and SD represent average and standard deviation, respectively.

3.1.2. Longitudinal Stress

In addition to determining the velocity of the longitudinal wave, it was also deemed of importance to track the stress developed behind the longitudinal wave front. Specifically, it was desired to probe the validity of Equations (2)–(6). As such, due to the use of force transducers required for camera triggering and longitudinal wave tracking, it became possible to track the force developed behind the longitudinal wave front when impacting at low velocities. This low velocity stipulation, being required by load cell restrictions, led to tracking of force levels developed due to the transverse impact of razor blade projectiles, as such sharp projectiles presented the lowest yarn critical velocity transition regime [12]. Two different yarn types were analyzed when impacting in the aforementioned loading conditions, namely Kevlar® KM2 and AuTx®, with resulting max tensile stress values as a function of impacting velocity shown in Figure 6. Stress values were calculated using the measured force and yarn cross-sectional areas found in Hudspeth et al. [18]. Additionally, the analytical stress described by Equations (2)–(6) has also been overlaid on both plots within Figure 6 (assuming $\sigma = \epsilon E_{avg}$, E_{avg} found in Table 2). It is important to note that the stress measured in the load cell is nearly twice that generated in the wake of the longitudinal wave, due to the wave reflection from the rigid clamp boundary. As such, the measured stress values shown in Figure 6 result from maximum detected load amplitudes that have been appropriately halved to represent the stress that would be developed behind the longitudinal wave front before interaction with the rigid clamping boundary. As shown in Figure 6, there can be seen a demonstrative drop in max stress within the critical velocity transition regime due to the immediate rupture of the constituent fibers.

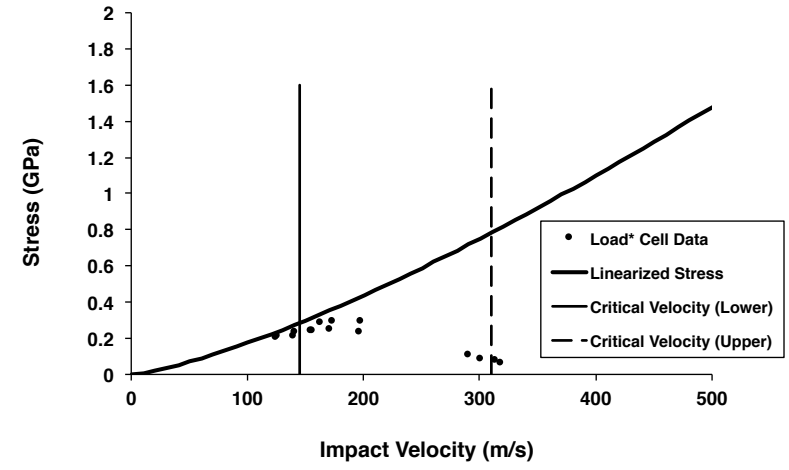

(a)

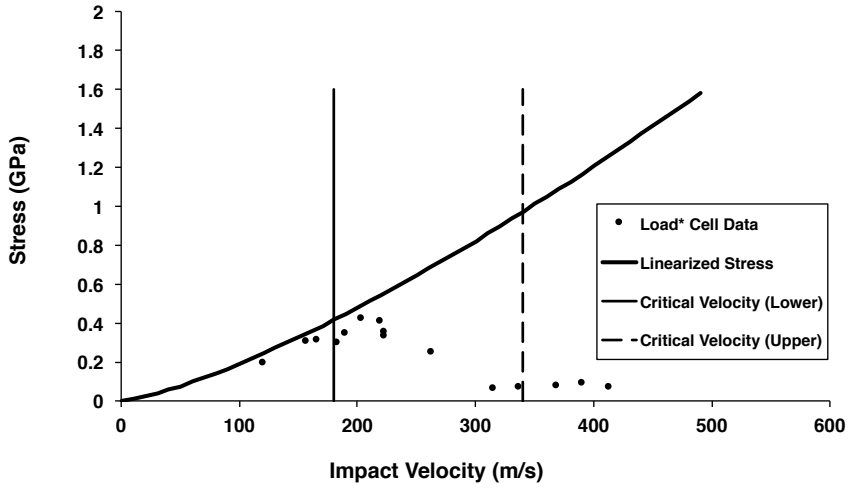

(b)

Figure 6. Longitudinal tensile stress developed behind the longitudinal wave front in both (**a**) Kevlar® KM2 and (**b**) AuTx® when impacted via razor blade projectiles. *Load data recorded from force transducers have been converted to stress assuming $\sigma = F/A$ wherein A is the cross-sectional area of the filaments within the tow using density and linear density values listed in Hudspeth et al. [18].

3.2. Transverse Wave Speed

In order to provide additional validity of Equations (2)–(6), it was deemed of use to track the transverse wave speed developed in yarn when subjected to transverse impact. As such, transverse wave speeds were analyzed via high-speed imaging of impact into AuTx® yarns using both FSP and round projectile heads. Implemented impact velocities spanned from roughly 400 m/s–1000 m/s. Below the critical velocity, wherein no filaments fail upon impact, impact via FSP and round projectile heads resulted in transverse wave speeds being quite close to those predicted from Equation (5). Examples of this impact event can be seen in Figures 7 and 8 when impacting with FSP and round projectiles, respectively. Both image sequences, which represent impacting velocities of 394 m/s (FSP) and 508 m/s (round), demonstrate experimental transverse wave velocities quite close to the their respective theoretical values, being 824 m/s compared to 832 m/s (FSP) and 960 m/s compared to 970 m/s (Round).

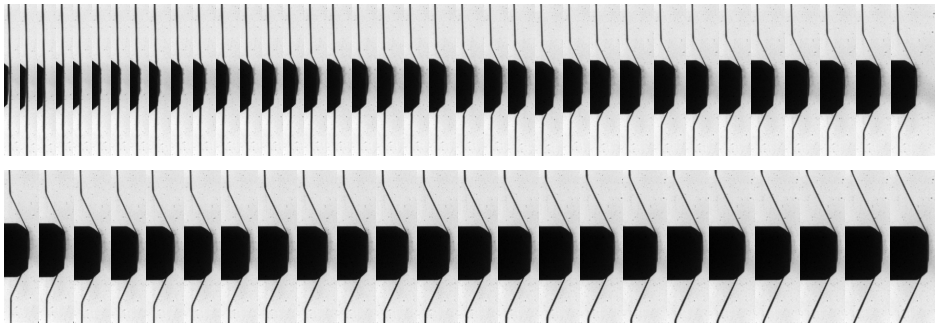

(a)

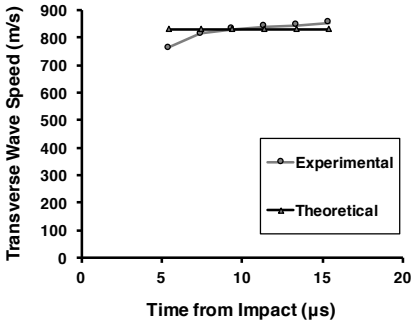

(b)

Figure 7. (**a**) Image sequence of an FSP transversely impacting into a single AuTx® yarn at 394 m/s (below critical velocity transition regime [12]), along with (**b**) corresponding measurement of transverse wave speed overlaid with the theoretical value predicted by Equation (5).

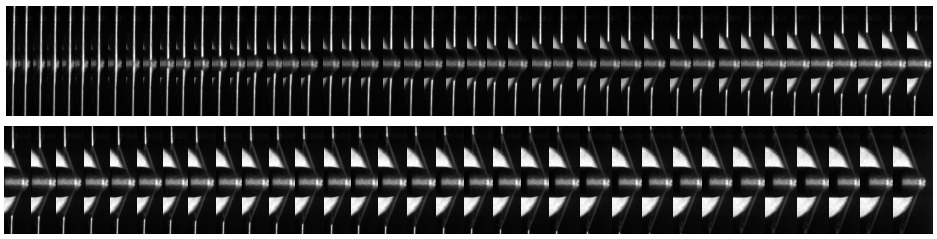

(a)

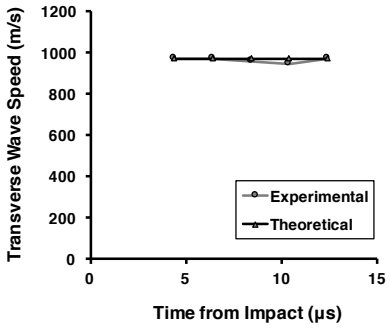

(b)

Figure 8. (**a**) Image sequence of a round projectile transversely impacting into a single AuTx® yarn at 508 m/s (below the critical velocity transition regime [12]), along with (**b**) corresponding measurement of transverse wave speed overlaid with the theoretical value predicted by Equation (5).

At higher impacting velocities residing within the critical velocity transition region, the lead transverse wave velocity again showed very good agreement to theoretical prediction, which can be seen in Figures 9 and 10 for 621 m/s (FSP) and 659 m/s (round) projectile impact, respectively. The measured experimental and predicted theoretical transverse wave velocities were 1142 m/s and 1093 m/s (FSP) and 1114 m/s and 1132 m/s (round), respectively. Interestingly, both projectiles clearly demonstrate the partial nature of failure when shooting within the critical velocity transition region [12], and a range of transverse wave velocities is detected, depending on the fail/no-fail status of each filament. Both Figures 9 and 10 also show a plot of the minimum measured transverse wave speed, thereby demonstrating the aforementioned variation in transverse wave speed. An example of the location exhibited by the minimum and maximum transverse wave speeds is demarcated in Figure 9 via $*$ and -, respectively. Said minimums have been measured as 223 m/s and 239 m/s for the FSP and round projectile impact conditions shown in Figures 9 and 10, respectively. It is important to note that the minimum and maximum measured wave speeds appear to be constant throughout the range of relevant image times.

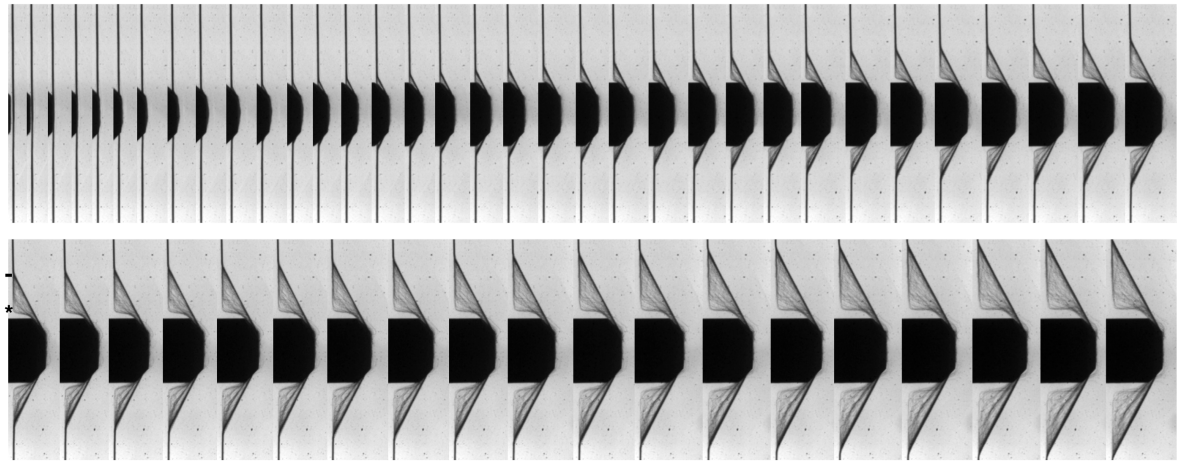

(a)

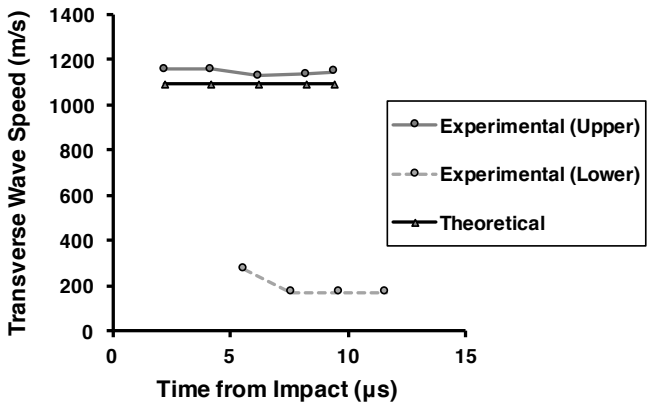

(b)

Figure 9. (**a**) Image sequence of an FSP transversely impacting into a single AuTx® yarn at 621 m/s (inside the critical velocity transition regime [12]), along with (**b**) corresponding measurement of transverse wave speed overlaid with the theoretical value predicted by Equation (5).

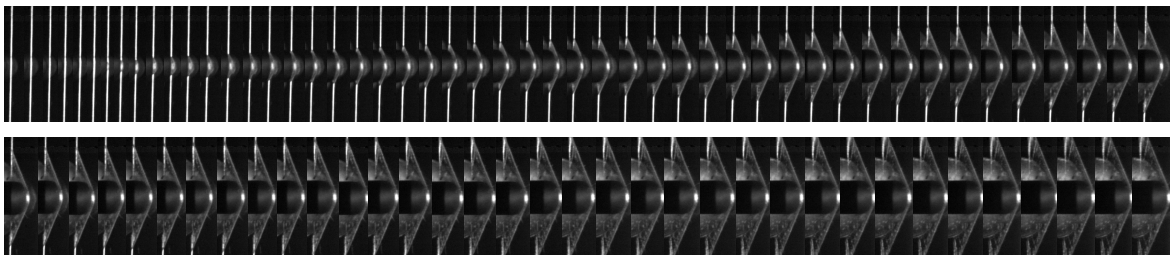

(a)

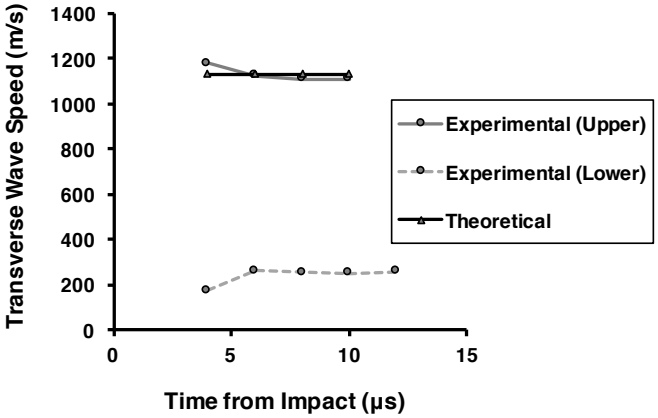

(b)

Figure 10. (**a**) Image sequence of a round projectile transversely impacting into a single AuTx® yarn at 659 m/s (inside the critical velocity transition regime [12]), along with (**b**) corresponding measurement of transverse wave speed overlaid with the theoretical value predicted by Equation (5).

Transverse wave speeds were also tracked from representative shots fired above the critical velocity transition regime for both FSP and round projectile geometries, which are shown in Figures 11 and 12. As opposed to the shots fired below and within the critical velocity transition regime, shots impacting above the critical velocity region do not express constant transverse wave velocities. Indeed, they show a progressive reduction in transverse wave speed with increasing time post projectile-yarn contact. For both the FSP and round projectile impact, the initial measured transverse wave velocity appears to correspond exceedingly well with the theoretical transverse wave velocities predicted from Equation (5). Initial measured transverse wave speeds and the theoretical wave speeds initiated via transverse impact were 1281 m/s and 1273 m/s (FSP) and 1316 m/s and 1433 m/s (round), respectively. The FSP impact velocity was measured to be 806 m/s, and the round impact velocity was measured to be 994 m/s. For both impact conditions, a stark drop in transverse wave speed can be seen in the measured time window, resulting in a transverse wave velocity of 748 m/s at 12.2 μs post impact and 749 m/s at 11.8 μs post impact, for the FSP and round projectile, respectively. As with the shots shown in Figures 9 and 10, there exists a range in the transverse wave speed due to partial yarn failure. The slowest moving broken filaments appear to possess a transverse wave speed of roughly 200–400 m/s, with this wave speed reducing in value as time post contact progresses. Again, it is reiterated that there exists a reduction in both maximum and minimum transverse wave speeds with progressing time post impact. Such a reduction in wave speed values is believed to signify the occurrence of progressive failure in the yarn; indeed, initial transverse wave speeds are quite similar to the corresponding theoretical transverse wave speed, demonstrating initially intact filaments, which is then followed by a reduction in demonstrated transverse wave speed due to complete filament failure. Thus, it is interesting to note that the "immediate" failure of a yarn is not indeed immediate. Rather, there is a slight window wherein both longitudinal and transverse waves are allowed to develop.

While the longitudinal wave is able to propagate outwards without a reduction in velocity at the wave front, the transverse wave, which must be fed by inflowing material behind the longitudinal wave front, is subject to the level of failure of the yarn upon impact. Below the critical velocity transition regime, the transverse wave is fed completely from the inflowing material behind the longitudinal wave front. Within the velocity transition regime, only intact filaments continue to provide the tension and inward flow characteristics needed to feed the transverse wave. Above the critical velocity transition regime, all yarn material fails, but not immediately upon impact, thereby allowing for an initial transverse wave to develop before rarefaction waves from failed filaments deplete the yarn longitudinal stress levels required for continued transverse wave propagation. Thus, yarn failure is not seen to be immediate within the impact conditions of the current experimental setup; rather, the failure process is seen to be progressive as the projectile moves through the bundled filaments in the transverse direction.

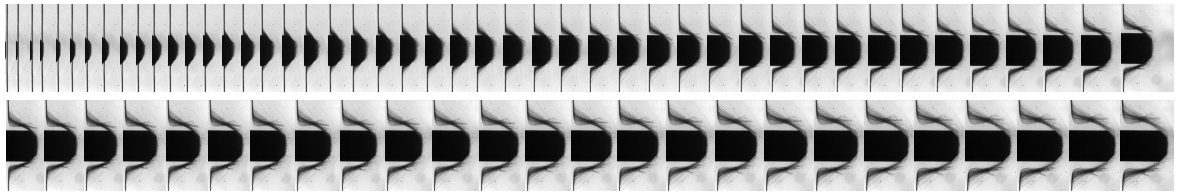

(a)

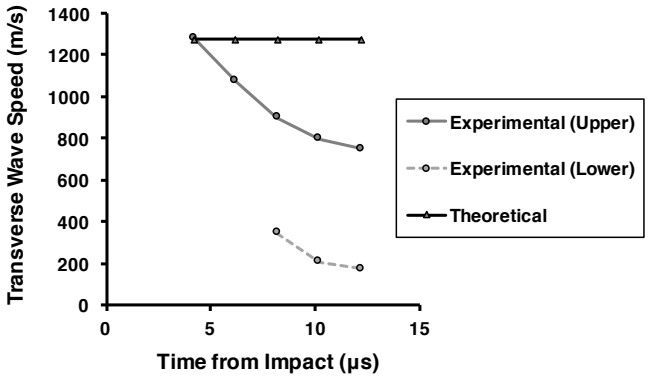

(b)

Figure 11. (**a**) Image sequence of an FSP transversely impacting into a single AuTx® yarn at 806 m/s (above the critical velocity transition regime [12]), along with (**b**) corresponding measurement of transverse wave speed overlaid with the theoretical value predicted by Equation (5).

Finally, transverse wave speeds measured from several experiments within the 400 m/s–1000 m/s velocity window were plotted against their corresponding impact velocity and can be found in Figure 13. As shown in the data presented in Figures 7–12, the transverse wave propagation measurement scheme was slightly different below, within and above the critical velocity transition regime. Below said regime, the transverse wave front was tracked as the entire yarn showed a stark "tent-like" deformation and stayed constant during the entire imaging history. Within the transition regime, a range of transverse wave velocities was measured due to partial yarn failure, and only the leading edge of the transverse wave front was used to calculate the wave speed presented in Figure 13. Above the transition regime, due to rapid failure of the entirety of the yarn, only early time calculations were used to determine the transverse wave velocities presented in Figure 13. Overlaid on top of the experimental transverse wave velocities in Figure 13 is also the theoretical transverse wave velocity as a function of the projectile impact speed. The experimentally-measured velocities correspond quite well with the theoretical transverse wave speed, bringing further verification to Equations (2)–(6).

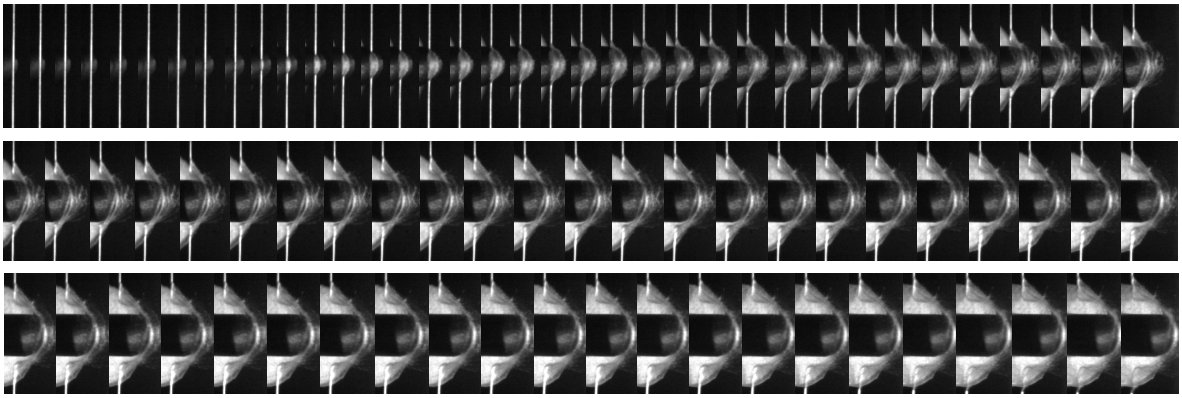

(a)

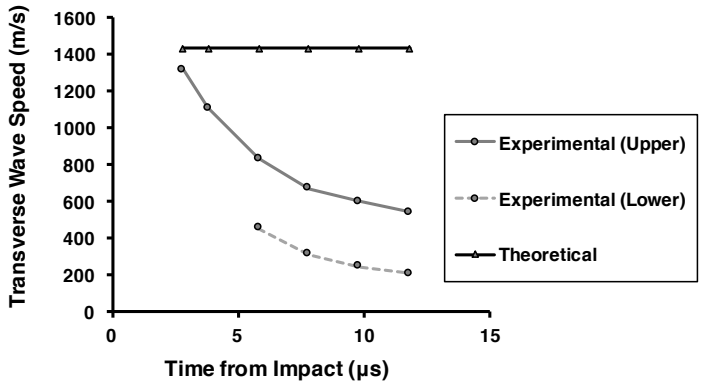

(b)

Figure 12. (**a**) Image sequence of a round projectile transversely impacting into a single AuTx® yarn at 994 m/s (above the critical velocity transition regime [12]), along with (**b**) corresponding measurement of transverse wave speed overlaid with the theoretical value predicted by Equation (5).

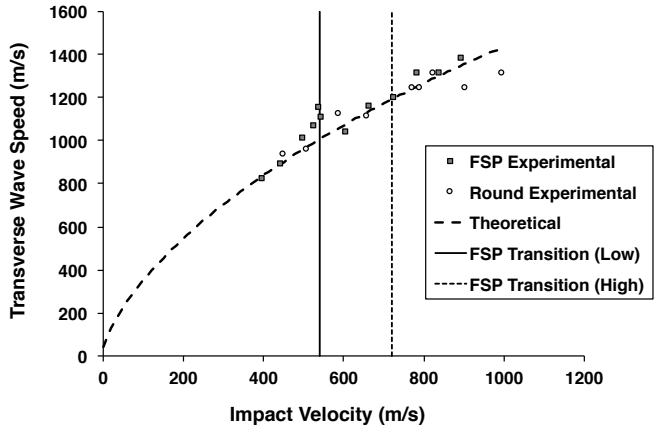

Figure 13. Experimental and theoretical transverse wave velocities for AuTx® yarn shot with both FSP and round projectile geometries.

4. Optimization of Filament Properties

Due to conjectures made regarding the optimization in the mechanical properties of high-performance filament material [19] and the governing constraints constituent yarn places on

the performance of an entire fabric system, a basic thought experiment has been performed to assess the effect of varying failure strength, failure strain and the elastic modulus of yarn material, both in controlling the resulting critical velocity as predicted by the Smith equations (Equations (2)–(7)) [20] and, even more importantly, the Cunniff parameter (1).

4.1. Constitutive Equation Modification

Due to the simultaneous solution requirement of Equations (2)–(6), said relations have been somewhat simplified via removing higher order strain terms. Such a simplification can be seen in the following:

$$W = c\epsilon \tag{11}$$

$$U = \sqrt{\frac{E}{\rho}\left(\frac{\epsilon}{1+\epsilon}\right)} \cong c\sqrt{\epsilon} \tag{12}$$

$$U_{obs} = c\left(\sqrt{\epsilon(1+\epsilon)} - \epsilon\right) \cong c\left(\sqrt{\epsilon} - \epsilon\right) \tag{13}$$

$$V = \sqrt{(1+\epsilon)^2U^2 - ((1+\epsilon)U - W)^2} \cong c\sqrt{2\epsilon\sqrt{\epsilon}} \tag{14}$$

In order to demonstrate the validity of Equations (12)–(14), all three relations have been solved for a range of impact velocities up to 1 km/s and are plotted in Figure 14 using mechanical properties exhibited by Kevlar® KM2. Figure 14a compares the full solution (6) and simplified solution (14) of the tensile strain developed behind the longitudinal wave front, showing very good agreement, with the simplified solution tending to be slightly less than the full solution. Figure 14b compares the variation in the full solution and simplified solution of the transverse wave speed in both a reference onboard the yarn (Equations (4) and (12), respectively) and from the reference of a laboratory observer (Equations (5) and (13), respectively). Both comparisons show very similar results between the full solution and simplified solution with the partial solution of U tending to slightly overpredict the full solution and the partial solution of U_{obs} tending to slightly underpredict the full solution. Thus, the following assessment of mechanical property evaluation on the resulting critical velocity uses the simplified set of equations for ease of analysis.

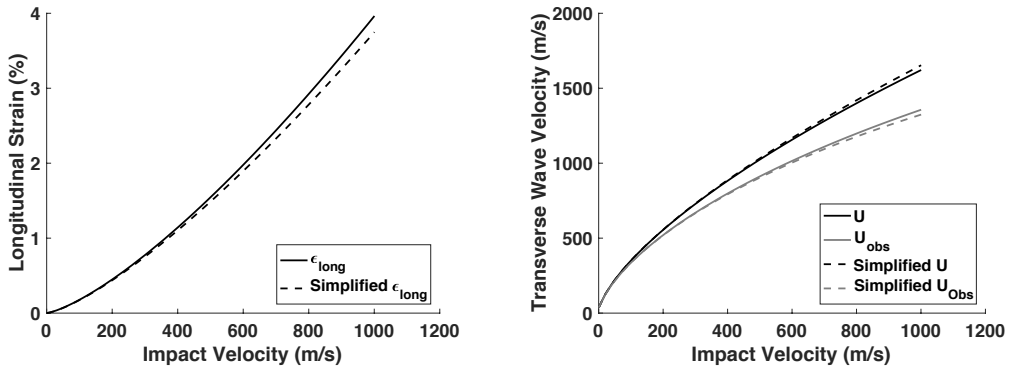

(a) (b)

Figure 14. Plots showing the variation in the full analytical solution and simplified solution of (**a**) the longitudinal strain and (**b**) the transverse wave speed developed during transverse impact for a Kevlar® KM2 yarn.

4.2. Material Property Modification: Single Yarn Critical Velocity

As it has been proposed that an increase in yarn critical velocity will result in a corresponding increase in full fabric performance, it is of interest to understand the coupled effect of increasing single

filament mechanical properties. Specifically, it is of interest to understand the effect of varying failure stress, failure strain and elastic modulus. As a first trial of single filament performance, it is of use to compare linear elastic mechanical parameters, considering the long-range tensile characteristics demonstrated at rupture. This analysis assumes a linear elastic response of the material; such an assumption is well substantiated from experimental evidence [21–23]. It must be noted that previous work has demonstratively shown that single filaments do not fail in pure tension [15,18], but this short analysis is solely being performed to elucidate the effect of local failure characteristics resulting in strength/strain increases measured during transverse loading.

In order to assess the effect of the coupled variation of failure strength and failure strain on the resulting yarn critical velocity, Equation (14) has been modified to remove the elastic modulus term, E, present within the yarn wave speed (c), thereby presenting the critical velocity, V, as a function of solely failure strain and failure stress. Said modification can be seen in Equation (15).

$$V = \sqrt{\frac{2}{\rho}\sigma\sqrt{\epsilon}} \tag{15}$$

An array of values of σ and ϵ are then input into Equation (15), yielding a critical velocity surface, which can be seen in Figure 15a. Additionally, iso-velocity curves have been overlaid on top of the velocity surface with curves ranging from 300 m/s–1000 m/s in 100-m/s increments. Take notice of the clear effect that both failure strain and failure stress have on the resulting critical velocity. Increasing either value while holding the other constant shows an increase in critical velocity, but simultaneous increases in both are clearly the most preferable.

In efforts to more easily visualize the effect of both failure stress and failure strain, Figure 15a has been reoriented to view along with the critical velocity axis, which can be seen in Figure 15b, using the same color scheme present in Figure 15a. As previously stated, there is clearly a coupled effect of increasing either the long-range failure stress or failure strain of the impacted yarn material, assuming a linear elastic response. The described plot contains iso-velocity lines for a filament material possessing a density of 1.45 g/cm^3. Overlaid on said plot can be seen an example failure stress/strain solution of a yarn exhibiting a critical velocity of 500 m/s. In this specific case, the failure stress and failure strain are ~1.48 GPa and 1.48%, respectively. Again, note that an increase in either failure property (failure stress or failure strain) while holding the neighboring parameter constant will result in an increase of the transverse impact critical velocity.

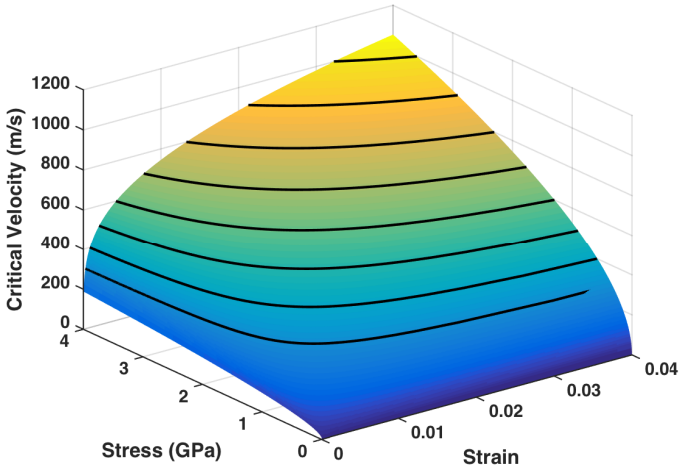

(a)

Figure 15. *Cont.*

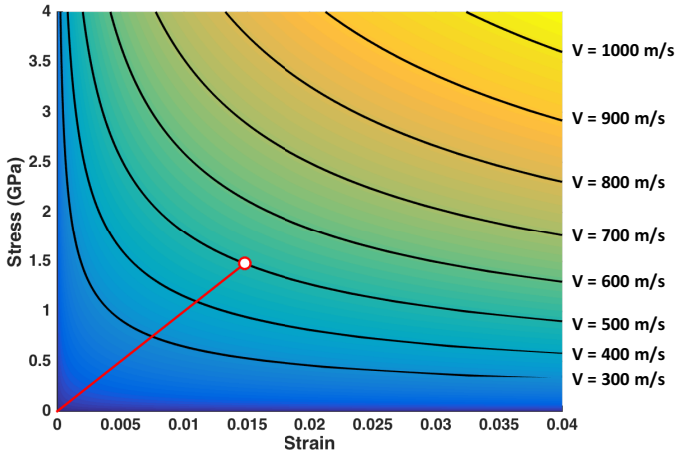

(b)

Figure 15. (**a**) Variation in the critical velocity ($V_{critical}$) of a single Kevlar® KM2 yarn subject to transverse impact when varying both the failure stress and failure strain of the yarn material. (**b**) Stress-strain field overlaid with critical iso-velocity curves; example linear elastic stress-strain response resulting in a critical velocity of 500 m/s.

From Equation (15), it can also be seen that changes in failure stress result in a more rapid increase (and decrease) in critical velocity, as compared to proportional changes in failure strain. For example, a 10% increase in failure stress results in a critical velocity of 524.4 m/s, while a 10% increase in failure strain results in a critical velocity of 512.1 m/s. Figure 16 demonstrates the variation in critical velocity due to the modification of either exclusively failure stress or exclusively failure strain.

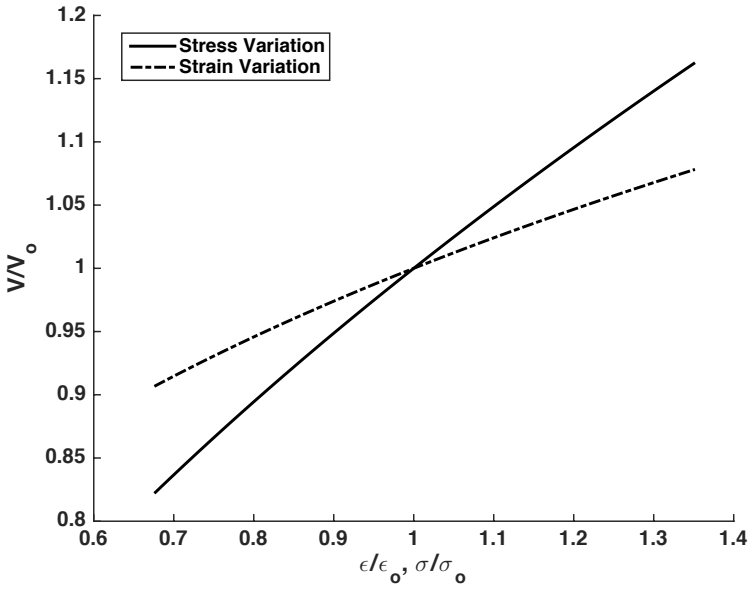

Figure 16. Relative effect of varying either the ultimate failure stress or failure strain of Kevlar® KM2 yarn on the resulting single yarn critical velocity, $V_{critical}$ (assuming an initial failure stress and failure strain of 1.48 GPa and 1.48%, respectively).

4.3. Material Property Modification: Cunniff Equation

Similar to the analysis performed on the simplified Smith equations given in the previous section, it was also deemed of use to analyze the effect of changes in mechanical properties on the resulting Cunniff parameter, shown previously in Equation (1). Equation (1) can be modified to be written as a function of either longitudinal wave speed and failure strain, longitudinal wave speed and failure stress or failure stress and failure strain. Such versions of the Cunniff parameter are shown in Equation (16). As previously mentioned, the first two equalities in Equation (16) were used by Phoenix and Porwal [19] in order to assess the effect that changing mechanical properties has on the resulting Cunniff parameter.

$$\Omega^{1/3} = c\left(\frac{\epsilon}{\sqrt{2}}\right)^{2/3} = c^{-1/3}\left(\frac{\sigma}{\sqrt{2}\rho}\right)^{2/3} = \sqrt{\frac{2^{-2/3}}{\rho}}\sigma^{1/2}\epsilon^{1/6} \tag{16}$$

The first inequality demonstrates the effect of varying either failure strain or wave speed. In this format, increases in ballistic performance are initially suggested to increase when there is either an increase in failure strain or longitudinal wave speed, which follows intuitive reason. In contrast, the second equality, which is manipulated to be a function of failure stress and longitudinal wave speed, suggests that either increases in failure stress or decreases in longitudinal wave speed will render increases in the resulting Cunniff parameter. Although formally correct, such a representation of the Cunniff parameter is somewhat misleading, and reasoning for the occurrence is the result of the failure stress having a greater effect on the Cunniff parameter as opposed to the failure strain, which is demonstrated by the third equality shown in Equation (16). Similar to the dataset shown for the Smith equation, it is of use to plot out the Cunniff parameter as a function of both failure stress and failure strain, which can be seen in Figure 17a. Additionally, iso-velocity lines have been overlaid on the surface plot of Figure 17b, ranging from 100 m/s–700 m/s in 100-m/s intervals. In an effort to more easily visualize the effect of failure stress and failure strain on the resulting Cunniff parameter, the surface plot of Figure 17a has been reoriented to view down the critical velocity axis, which is depicted in Figure 17b. Iso-velocity lines similar to those depicted in Figure 17a have also been overlaid on Figure 17b.

Using Figure 17 and Equation (16), it is now of interest to assess the effect of elastic material property variation. A linear elastic stress-strain curve having a modulus of 100 GPa has been overlaid on Figure 17b, which shows a Cunniff parameter of 400 m/s, resulting in a failure stress and failure strain of 1.49 GPa and 1.49%, respectively. Clearly an increase in either failure stress or failure strain will provide an increase in ballistic performance, but increases in failure stress demonstrate a greater effect than proportional changes in failure strain; this effect can be seen in Figure 18a, wherein a 10% increase in solely failure strain or a 10% increase in solely failure stress exhibits a Cunniff parameter increase of 1.6% and 4.9%, respectively. Additionally, Figure 18b demonstrates that the Cunniff parameter is more strongly affected by variations in the yarn toughness while holding the elastic modulus constant as compared to varying the elastic modulus while holding the toughness constant, which is readily seen from the native version of the Cunniff equation (Equation (1)).

Examining Equation (16), it is of use to discuss the means of increasing the Cunniff parameter, thereby increasing the ballistic resistance of a soft-armor system. The simplest positive governance of the Cunniff parameter entails a decrease in material density while keeping mechanical properties constant; such a result is any material scientist's prized outcome, but is typically unattainable, as a fiber manufacturer is generally only able to alter mechanical response within a specific material class (e.g., working on an aramid or ultra-high molecular weight polyethylene fiber). Thus, in efforts to still provide an increase to the Cunniff parameter, the material scientist is sequestered within mechanical property alteration. Equalities listed in Equation (16) demonstrate several mechanical property relationships, assuming a linear elastic material response. Of course, all three of these Cunniff parameter variants are valid, but caution is suggested to the reader to remember the inherent meaning of the parameter's original form. It is again reiterated that the Cunniff parameter is most

meaningfully described in its native state as the product of yarn toughness and longitudinal wave speed; an improved yarn material will transport energy away from the impact site more rapidly and can withstand greater loading environments.

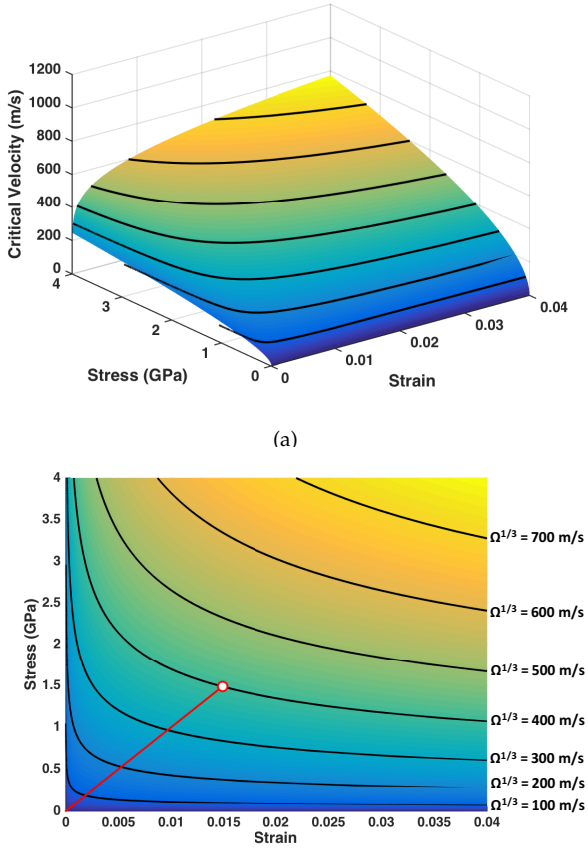

(a)

(b)

Figure 17. (**a**) Variation in the Cunniff parameter, $\Omega^{1/3}$, when varying both the failure stress and failure strain of Kevlar® KM2 yarn material. (**b**) Stress-strain field overlaid with critical iso-velocity curves; example linear elastic stress-strain response resulting in a Cunniff parameter of 400 m/s.

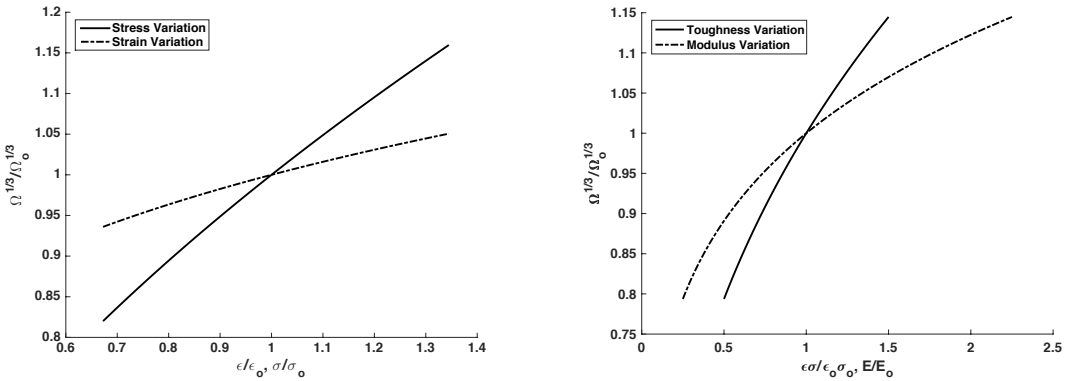

(a)

(b)

Figure 18. Relative effect of varying (**a**) the ultimate failure stress or failure strain or (**b**) the toughness or elastic modulus on the resulting Cunniff parameter, $\Omega^{1/3}$, for Kevlar® KM2 yarn (assuming an initial failure stress and failure strain of 1.49 GPa and 1.49%, respectively).

4.4. Material Property Modification: Comparison of Smith and Cunniff Equations

Finally, it is of use to compare both the Smith equation and the Cunniff equation in the format shown in Equations (17) and (18).

$$V = \sqrt{\frac{2}{\rho}}\sigma^{1/2}\epsilon^{1/4} \tag{17}$$

$$\Omega^{1/3} = \sqrt{\frac{2^{-2/3}}{\rho}}\sigma^{1/2}\epsilon^{1/6} \tag{18}$$

Interestingly both equations are very similar in nature, with the Cunniff equation being slightly less controlled by the failure strain than the Smith equation. The similarity of these equations can also be verified by the plots shown in Figures 15 and 17. It is thus suggested that very similar understanding can be gained from finding the yarn critical velocity by performing single yarn impact experiments as compared to shooting entire armor systems in efforts to determine V_{50} values. Used as a preliminary design tool, the former experiment is much less costly to perform, and analysis can be performed on small batches of material developed either from desktop-made filaments or from pilot runs on an experimental fiber spinning line.

5. Conclusions

Initial portions of this work were directed at performing single yarn transverse impact experiments in an effort to gain understanding of waves developed due to the impact event. Firstly, longitudinal wave speeds were tracked in Kevlar® KM2 and Dyneema® SK76 in order to back-out material stiffness, with the desire to detect the presence of material rate sensitivity. Three different projectile nose geometries were used to impact the yarn material, namely razor blade, FSP and round. Slightly differing wave speeds were detected from the three different projectile nose geometries, not due to the nose geometry itself, but rather because of the differing strike velocities used for each nose geometry. As these experiments were performed in efforts to uncover the yarn critical velocity [12], increasing impact velocities were required to promote immediate rupture for the razor blade, FSP and round nose geometries, respectively, due to the corresponding increase in stress concentration for the three projectile heads. Longitudinal wave speed measurements were also used to detect the max load developed in Kevlar® KM2 and AuTx® yarn behind the longitudinal wave front, which agreed very well with theory. Subsequently, transverse wave speeds were measured for AuTx® yarns for a variety of impacting velocities, which also agreed quite well with theory. Effort was also placed in understanding the transverse wave development around the yarn critical velocity. Below the critical velocity, the transverse wave demonstrated full yarn transverse displacement with a constant transverse wave speed. Within the critical velocity transition region, partial yarn failure was detected, resulting in a range of transverse wave speeds exhibited by the material; the leading edge of the transverse wave was constant and moved with the theoretically-predicted velocity. The slowest moving transverse wave, though constant in the region measured, was much slower than the leading edge, presumably due to the lack in tension from filament failure. Above the critical velocity, the entire yarn failed, but measurement of the initial leading edge of the transverse wave yielded a transverse wave velocity similar to that predicted from theory. With time progression, the leading edge (and the trailing edge) of the transverse wave decreased in velocity.

Finally, effort was directed towards understanding room for filament improvement, demonstrating that common linear-elastic, high-performance polymer fiber promote greater increases in ballistic performance (both the Cunniff parameter and the Smith single yarn critical velocity) with increases in yarn toughness or elastic stiffness, although the former yields greater performance effects than the latter. Additionally, it was determined that changes in failure stress are more significant than changes in failure strain for these common fiber types. Due to the similarity between the Cunniff parameter and the critical velocity arising from the Smith equations, effort has also been directed

toward warning the reader to be wary of manipulating the Cunniff equation in a way to show that decreases in wave speed can actually improve ballistic performance. Although correct in certain modifications of failure stress, such a claim is actually identical to suggesting an increase in yarn toughness, which as previously mentioned, is more powerful at controlling the Cunniff parameter than the elastic stiffness.

Acknowledgments: The authors would like to thank experimental design efforts from Ben Claus and Boonhim Lim. The authors must also thank Phil Jewell in his experimental assistance. M.H. would like to thank financial support from the National Defense Science and Engineering Fellowship. M.H. would also like to thank Sidney Chocron of Southwest Research Institute for kindly providing access to the Wang et al. [16] study.

Author Contributions: M.H. and W.C. conceived and analyzed experiments and contributed in discussion. M.H. and E.J. performed experiments. J.Z. and S.H. supervised project direction and contributed in discussion.

Conflicts of Interest: The authors declare no conflict of interest. The founding sponsors had no role in the design of the study; in the collection, analyses or interpretation of data; in the writing of the manuscript; nor in the decision to publish the results.

References

1. Petterson, D.; Stewart, G.; Odell, F.; Maheux, R. Dynamic distribution of strain in textile materials under high-speed impact: Part I: Experimental methods and preliminary results on single yarns. *Text. Res. J.* **1960**, *30*, 411–421.
2. Smith, J.C.; Fenstermaker, C.A.; Shouse, P.J. Stress-Strain Relationships in Yarns Subjected to Rapid Impact Loading: Part X: Stress-Strain Curves Obtained by Impacts with Rifle Bullets. *Text. Res. J.* **1963**, *33*, 919–934.
3. Wilde, A.; Ricca, J.; Roger, J. Breaking energies of a nylon series subjected to high-speed transverse impact. *Polym. Eng. Sci.* **1972**, *12*, 41–47.
4. Freeston, W.; Platt, M.; Coskren, R. The stress-strain response of yarns at high rates of loading. *Int. Text. Inst.* **1972**, *63*, 239–262.
5. Claus, W.; Donovon, J.; Freeston, W. *Devaluation of the Mechanical Properties of Yarns for Ballistic Applications*; Technical Report 73-60-CE; Fabric Research Laboratories: Dedham, MA, USA, 1973.
6. Abbott, N.; Donovan, J.; Schoppee, M. *The Effect of Temperature and Strain Rate on the Tensile Properties of Kevlar and PBI Yarns*; Technical Report AFML-TR-65, Part II; Fabric Research Laboratories: Dedham, MA, USA, 1974.
7. Coskren, R.; Abbott, N.; Ross, J. Kevlar 29 parachute fabrics. In Proceedings of the AIAA Aerodynamic Deceleration Systems Conference, Albuquerque, NM, USA, 17–19 November 1975; pp. 1–6.
8. Carr, D.J. Failure Mechanisms of Yarns Subjected to Ballistic Impact. *J. Mater. Sci. Lett.* **1999**, *18*, 585–588.
9. Bazhenov, S.L.; Dukhovskii, I.A.; Kovalev, P.I.; Rozhkov, A.N. The Fracture of SVM Aramide Fibers Upon a High-Velocity Transverse Impact. *Polym. Sci. Ser. A* **2001**, *1*, 61–71.
10. Chocron, S.; Kirchdoerfer, T.; King, N.; Freitas, C.J. Modeling of Fabric Impact With High Speed Imaging and Nickel-Chromium Wires Validation. *J. Appl. Mech.* **2011**, *78*, 051007.
11. Cunniff, P. Dimensionless Parameters for Optimization of Textile-Based Body Armor Systems. In Proceedings of the 18th International Symposium on Ballistics, San Antonio, TX, USA, 15–19 November 1999; Volume 2, pp. 1303–1310.
12. Hudspeth, M.; Chu, J.; Jewell, E.; Lim, B.; Ytuarte, E.; Tsutsui, W.; Horner, S.; Chen, J.Z.W. Effect of projectile nose geometry on the critical velocity and failure of yarn subjected to transverse impact. *Text. Res. J.* **2016**, *87*, doi:10.1177/0040517516646040.
13. Walker, J.D.; Chocron, S. Why Impacted Yarns Break at Lower Speed Than Classical Theory Predicts. *J. Appl. Mech.* **2011**, *78*, 051021.
14. Sockalingam, S.; Gillespie, J.; Keefe, M. Dynamic modeling of Kevlar KM2 single fiber subjected to transverse impact. *Int. J. Solids Struct.* **2015**, *67–68*, 297–310.
15. Hudspeth, M.; Chen, W.; Zheng, J. Why the Smith theory over-predicts instant rupture velocities during fiber transverse impact. *Text. Res. J.* **2015**, doi:10.1177/0040517515586158.
16. Wang, L.L.; Field, J.E.; Sun, Q. Dynamic Behaviour of Prestressed High Strength Polymeric Yarns Transversely Impacted by a Blade. In Proceedings of the International Symposium on Intense Dynamic Loading and Its Effects, Chengdu, China, 9–12 June 1992; pp. 354–359.

17. Cansfield, D.; Ward, I.; Woods, D.; Buckley, A.; Pierce, J.; Wesley, J. Tensile strength of ultra high modulus linear polyethylene filaments. *Polym. Commun.* **1983**, *24*, 130–131.
18. Hudspeth, M.; Li, D.; Spatola, J.; Chen, W.; Zheng, J. The effects of off-axis transverse deflection loading on the failure strain of various high-performance fibers. *Text. Res. J.* **2015**, *86*, doi:10.1177/0040517515588262.
19. Leigh Phoenix, S.; Porwal, P.K. A new membrane model for the ballistic impact response and V50 performance of multi-ply fibrous systems. *Int. J. Solids Struct.* **2003**, *40*, 6723–6765.
20. Smith, J.C.; McCrackin, F.L.; Schiefer, H.F. Stress-Strain Relationships in Yarns Subjected to Rapid Impact Loading: Part V: Wave Propagation in Long Textile Yarns Impacted Transversely. *Text. Res. J.* **1958**, *28*, 288–302.
21. Cheng, M.; Chen, W.; Weerasooriya, T. Mechanical Properties of Kevlar®KM2 Single Fiber. *J. Eng. Mater. Technol.* **2005**, *127*, 197–203.
22. Lim, J.; Zheng, J.Q.; Masters, K.; Chen, W.W. Effects of gage length, loading rates, and damage on the strength of PPTA fibers. *Int. J. Impact Eng.* **2011**, *38*, 219–227.
23. Lim, J.; Zheng, J.Q.; Masters, K.; Chen, W.W. Mechanical behavior of A265 single fibers. *J. Mater. Sci.* **2010**, *45*, 652–661.